

Chapter 3

A Longwave Radiative Transfer Scheme for Climate Modelling and its Evaluation with Surface Observations at Cabauw

Abstract

We present a wide band longwave radiative transfer scheme, as an extension of the *Morcrette* [1989] code, in which all relevant atmospheric absorbers are included to be suitable for climate modelling. We evaluate this scheme with surface radiation measurements at Cabauw in the Netherlands for 253 clear sky hours during the period 1995-1996. As input for the scheme we combine the atmospheric profiles of temperature and humidity from the Cabauw tower (200m) with rawind sonde measurements at De Bilt. Total ozone data are derived from the Brewer spectrophotometer and used for scaling the Mid-Latitude Summer vertical ozone distribution. For a large range of measured downward longwave irradiances, between 180 and 360 Wm^{-2} , we find a correlation coefficient of 0.99. The bias of only -2 Wm^{-2} and the standard deviation of 4.2 Wm^{-2} are both within the range of the measurement errors. The transmission functions of the wide band scheme are determined from fits to narrow band model results in which temperature and pressure dependencies are taken into account. We use a statistical approach to process spectroscopic line parameters into transmission functions in the narrow band model. Three spectroscopic compilations are considered here, namely HITRAN 1980, GEISA 1984, and the most recent one, HITRAN 1996. Outputs in terms of heating rates and irradiances are discussed using reference atmospheres for clear-sky conditions. Differences up to 5 Wm^{-2} in the net irradiance at the tropopause are found by using either HITRAN 1980 and GEISA 1984, while differences between the latter and HITRAN 1996 appear to be one order of magnitude less. The same holds for the differences in heating rates, namely of the order 0.1 K/day and 0.01 K/day, respectively. Further parameterization of atmospheric radiative transfer towards the wide band scheme introduces errors of the order of 0.05 K/day. In addition, we have tested two formulations of the water vapour continuum, resulting in a difference of 12.5 Wm^{-2} using the 253 clear sky cases. Therefore, improvement can be accomplished by increasing the spectral resolution as well as the water vapour continuum formulation in schemes for climate modelling purposes.

¹R. van Dorland, P. Stammes, A.A.M. Holtslag, and W. Kohsiek, submitted to *Quart. J. Roy. Met. Soc.*, 1999.

3.1 Introduction

Radiation is one of the important features in the climate system. The only significant source of energy for this system is the shortwave radiation originating from the sun, while the longwave radiation emitted to space acts as a sink of energy. All scenarios regarding climate change are directly or indirectly based on radiative feedback mechanisms. From this point of view it will be clear that an accurate parameterization of the radiative processes in the atmosphere and at the Earth's surface is essential for climate modelling.

As stated by the Intercomparison of Radiation Codes for Climate Models (ICRCM) study group, one of the causes for uncertainty in the derivation of radiative fluxes and related quantities are the significant uncertainties in the spectral absorption parameters [Ellingson and Fouquart, 1990; IPCC, 1994]. Typically, calculations are performed with a cascade of radiative transfer models, ranging from the Line By Line (LBL) models, which resolve the actual line spectrum, the Narrow Band Models (NBM), which account for the transmission functions in a statistical sense, to the highly parameterized Wide Band Models (WBM), which are sufficiently computationally efficient to be incorporated in General Circulation Models e.g. Climate Models.

In this study, we aim to develop a longwave wide band radiative transfer scheme for climate modelling purposes. The basic version of the WBM is taken from Morcrette [1989] and extensions are made to include CH₄, N₂O, 16 CFCs, HCFCs and HFCs, as well as the 14 μm band of O₃ [Shine *et al.*, 1995]. The transmission functions for each absorber in the six WBM spectral intervals are determined from fits to NBM results in which temperature and pressure dependencies are taken into account, following the method of Morcrette *et al.* [1986]. These spectral intervals correspond to the scale of the unresolved band contours of the most important absorbers.

In the NBM, irradiances are computed in relatively small intervals. In these 225 spectral bands the Planck function may be considered as constant, while enough lines are positioned within such intervals to compute average transmission properties from spectroscopic line parameters using statistical band models. However, the calculation of these averaged parameters, especially the selection of the adopted random band model and the parameters describing the temperature dependencies, may introduce inaccuracies. Moreover, the use of these band models in combination with the choice of the spectral interval width must be guided by LBL calculations or accurate laboratory data [Ellingson *et al.*, 1991]. Although LBL models are often considered as benchmarks, some inaccuracies may be introduced by the fact that the cumulative contributions of wings of strong distant lines are not taken into account.

Here we compare three spectroscopic compilations: HITRAN (before: AFGL) 1980 [Rothman, 1981], GEISA 1984 [Husson *et al.*, 1986] and the HITRAN 1996 [Rothman, 1998]. The most recent spectroscopic dataset, HITRAN 1996, contains information over 360,000 lines corresponding to the five most important greenhouse gases, H₂O (4 isotopes), CO₂ (8 isotopes), O₃ (3 isotopes), N₂O (5 isotopes) and CH₄ (3 isotopes) in the considered spectral range 0 to 2820 cm⁻¹. Over a period of almost two decades, laboratory measurements of absorption lines have improved

considerably. First, the number of lines have increased. Large updates have been accomplished for ozone and methane as compared to the HITRAN 1980 database. Furthermore, spectroscopists have put effort in laboratory measurements of the temperature dependencies of the half-widths. For many lines, this became available since the GEISA 1984 edition [Chedin *et al.*, 1986]. For these spectroscopic compilations a direct comparison is made by computing mean absorption coefficients in the weak- and strong line absorption limits. In order to test the impact of the different spectroscopic line parameters on atmospheric longwave radiative transfer, we perform NBM experiments using the five clear-sky reference atmospheres [McClatchey *et al.*, 1972]. Additionally, the impact of the individual species has been tested using the Mid Latitude Summer (MLS) reference atmosphere, as recommended by ICRCCM [Ellingson and Fouquart, 1990].

Finally, WBM calculations are compared with radiation measurements at the Cabauw site in the Netherlands. We use clear-sky profiles of temperature and humidity, measured at Cabauw (200m) and rawind sonde data of De Bilt (nearest site), as well as total column ozone observations using a Brewer instrument, as input for the radiation scheme. We select 253 clear sky cases during the TEBEX (Tropospheric Energy Budget EXperiment) period (1995-1996) [Van Lammeren *et al.*, 1998], for which the measured downward longwave irradiance at the surface ranges by a factor of two from 180 to 360 Wm⁻². Several sensitivity tests are performed, i.e. the impact of possible errors in the measured atmospheric profiles and the use of different spectroscopic datasets, parameterized for the WBM. Special attention is paid to the water vapour continuum formulation, which is an important factor in particular for the counterradiation at the surface. We compare the formulation of Roberts *et al.* [1976], previously used in the ECMWF weather forecast system, with the more recent formulation developed by Ma and Tipping [1992], used in our WBM. Conclusions are made by comparing these differences with the typical errors in radiation measurements.

3.2 Theory and Background

3.2.1 Longwave Radiative Transfer

Radiative transfer calculations within atmospheric circulation models for weather and climate aim to compute the heating rate, i.e. the rate of temperature (T) change due to vertical divergence of the net irradiance:

$$\frac{\partial T}{\partial t} = \frac{g}{c_p} \frac{\partial F}{\partial p}, \quad (3.1)$$

where g is the acceleration due to gravity, c_p is the heat capacity of air at constant pressure, and F is the net irradiance at pressure level p . By virtue of the characteristic temperatures of the sun and the earth, solar ($<4\mu\text{m}$) and terrestrial ($>4\mu\text{m}$) radiative transfer can be separated quite well. Here, we focus on the infrared radiation. In this spectral region, radiation is attenuated due to absorption by greenhouse gases, while emission by the same gases result in a source term. Under assumption of local thermodynamic equilibrium, the source function equals the Planck

function (B_ν). Assuming further a non-scattering atmosphere and horizontal homogeneity, the two-stream radiative transfer equations (i.e. after integration over the zenith angles in two half spheres) can be written as [Goody and Yung, 1989]:

$$F_\nu^u(p) = [B_\nu(T_s) - B_\nu(T_a)]\tau_\nu(p, p_s; r) + B_\nu(T_p) + \int_p^{p_s} \tau_\nu(p, p'; r) \frac{d(B_\nu)}{dT} \frac{dT}{dp'} dp' \quad (3.2)$$

$$F_\nu^d(p) = [B_\nu(T_t) - B_\nu(T_\infty)]\tau_\nu(0, p; r) - B_\nu(T_p) + \int_0^p \tau_\nu(p', p; r) \frac{d(B_\nu)}{dT} \frac{dT}{dp'} dp', \quad (3.3)$$

where the subscripts u and d denotes the upward and downward components of the monochromatic irradiance (F_ν) at wavenumber ν , respectively, B_ν is the Planck function (in terms of irradiance), T is the temperature (where the subscripts refer to the surface (s), surface air (a), the model top of atmosphere (t), incident at top of atmosphere (∞) and the pressure level (p)), and $\tau_\nu(p', p; r)$ is the monochromatic (diffuse) transmission function of the irradiance through a slab between pressure levels p and p' . The latter is evaluated in a direction θ to the vertical such that $r = \sec \theta$ is the diffusivity factor or the reciprocal cosine of the representative zenith angle:

$$\tau_\nu(p, p'; r) = \exp\left[-r \int_{z(p)}^{z(p')} k_\nu(z') du(z')\right]. \quad (3.4)$$

Here k_ν is the absorption coefficient (in $\text{cm}^2 \text{g}^{-1}$) and $u(z)$ is the absorber amount (in g cm^{-2}). Difficulties in solving the longwave radiative transfer equations arise due to four integrations involved, namely integration over all zenith angles, vertical integration, spectral integration, and integration over inhomogeneous absorption path. In order to achieve sufficient accuracy in numerical computations of the irradiances, the last two integrals ought to be parameterized in a coupled way due to the large variation of line intensities depending strongly on temperature and pressure, while these entities as well as the absorber amount itself vary along the absorption path. Note that Eqs.3.2 and 3.3 are coupled in case of a partly reflecting surface for longwave radiation. Here, we use a reflection coefficient of 0.004.

3.2.2 Description of the Narrow Band Scheme

In the NBM, taken from *Morcrette and Fouquart* [1985], the longwave spectrum is divided into 225 spectral intervals, which are small enough (2 to 40 cm^{-1}) to regard the Planck function as constant across the intervals. The frequency averaged transmissivities are computed with the help of random band models, which are evaluated with the spectroscopic line parameters in combination with the (pressure scaled) absorber amount following *Rodgers and Walshaw* [1966]. These parameters are the ratio of the mean line intensity and mean line distance at 250 K, the line structure parameter at 250 K, including the half widths, and four coefficients of their temperature dependencies for each of the 225 frequency intervals. The processing of the spectroscopic entities for the greenhouse gases H_2O , CO_2 , O_3 , N_2O and CH_4 is described in the

Appendix. Two combinations of parameters occur in these transmissivity formulations, being the absorption coefficients in the limiting cases: G_{WLA} , the weak line approximation, depending on the line strengths only, and C_{SLA} , the strong line approximation, depending on both the line strengths and the collision half-widths.

Besides the five main greenhouse gases, we incorporate the absorption coefficients of 16 CFCs, HCFCs and HFCs. The line intensities of these heavy molecules are generally very strong, resulting in hardly any temperature dependencies. Multiplication of these line strengths with their relatively small abundances in the atmosphere result in small optical thicknesses. Therefore, the absorption regime of CFCs can be considered as rather weak. Band absorptances have been taken from the *AFEAS* [1989] report. Also, we modify the water vapour continuum formulation. The most favoured hypothesis assumes that the continuum is generated by the overlapping outer wings of the water vapour lines [Nordstrom and Thomas, 1980; Clough et al., 1989; Ma and Tipping, 1992]. It is found that the line shape of these wings show anomalies as compared to the Lorentzian line shape. Such a line shape is based on the assumption that the time between the collisions is much longer than the time spent during the collisions, which does not hold for water vapour. The continuum absorption consists of the e-type, which is proportional to the water vapour pressure, and the (p-e)-type, expressing the proportionality to the total pressure of all other atmospheric constituents. In the original code [Morcrette and Fouquart, 1985] the (p-e) type is a constant fraction ($\gamma=0.002$) of the e-type strength, following Roberts et al. [1976]. Ma and Tipping [1992] suggested a spectral dependence of this ratio (γ_v) on the basis of quantum mechanical calculations. Their formulation show a large effect for wavenumbers below 800 cm^{-1} . The continuum contributes substantially to the total irradiance, especially in the vicinity of the Earth's surface due to the water vapour distribution. In section 3.5.3 we will show the impact of the two formulations in the WBM.

3.2.3 Spectroscopic Datasets

In this study, we investigate the impact on atmospheric radiative transfer using the spectroscopic compilations of HITRAN 1980, GEISA 1984 and HITRAN 1996. A direct comparison of the line parameters of investigated datasets can be obtained by considering the Weak Line Approximation (WLA) and Strong Line Approximation (SLA) absorption coefficients at a reference temperature of 250 K for each absorber. Therefore, longwave spectral average values of the WLA and SLA absorption coefficients have been computed. Because in radiative transfer computations the transmissivities are weighted with either the Planck function B_ν or its temperature derivative dB_ν/dT (see Eqs.3.2 and 3.3), the averaged absorption coefficients, $\langle C(k) \rangle$, should include weighting factors w_j :

$$\langle C(k) \rangle = \frac{\sum_j w_j C(k_j)}{\sum_j w_j}, \quad (3.5)$$

where summations are carried out over all narrow band intervals j within wide band interval k , w_j is the weighting factor for spectral interval j and $\langle C(k) \rangle$ is the average absorption coefficient (WLA or SLA) in interval k . It is possible, with w_j being ΔB_j or $\Delta(dB/dT)_j$, to compute the impact of the differences between the spectroscopic compilations for absorbers in the weak line limit under isothermal conditions, since in this case averaged WLA coefficients are approximately proportional to averaged transmissivities. In all other (isothermal) cases, the weighting procedure is very complex, because WLA and SLA coefficients cannot be treated separately and absorber amounts and pressure effects have to be taken into account. On the other hand, if absorption coefficients are weighted with the width of the spectral interval (w_j being $\Delta\nu_j$), too much emphasis is put on the wings of the infrared spectrum, where the energy flux is small in comparison with the atmospheric window region. Nevertheless, by weighting with $\Delta\nu_j$ we get the average differences over the investigated spectrum.

In Table 3.1 we have listed the weighted averages of the WLA and SLA absorption coefficients computed for the HITRAN 1996 database and the relative differences herein for all possible permutations of the three spectroscopic compilations. We find that differences between the two oldest databases are generally larger than between GEISA 1984 and HITRAN 1996. However, we find large increases for the SLA-coefficient of ozone in the most recent database, reflecting the addition of many lines and half-width measurements in the nineties [Pinnock and Shine, 1998]. Differences for linear spectral weighting are larger by a factor of 1.5 than those for B and dB/dT weighting, indicating that most of the updates were in the wings of the longwave spectrum. The greenhouse effect of ozone is largely due to the 9.6 and 14 μm bands. Some weak lines have been added in these regions. The much larger absorption coefficients of CH_4 in the GEISA 1984 (65%) as well as the HITRAN 1996 (68%) compilations are mainly the result of missing lines in the wings of the 7.7 μm band contour in HITRAN 1980.

Differences in terms of atmospheric radiation are the result of changes in measured absorption coefficients combined with the abundances of the greenhouse gases for typical temperature profiles, e.g. in the five reference atmospheres. Therefore, changes in spectroscopic data of H_2O and CO_2 contribute most to differences in total atmospheric transmissivity. Their optical depths reach large values in most parts of the longwave spectrum, with the exception of the window region between 8 and 12.5 μm and in the vicinity of the 25 μm region. Therefore, differences in C_{SLA} give the best estimate for the changes in atmospheric radiation. For H_2O , the GEISA 1984 database gives the highest transmission and HITRAN 1980 the lowest transmission, although the SLA differences are quite dependent on the weighting procedure (Table 3.1). For CO_2 , the transmission at 250 K is lowest in HITRAN 1980 and about the same in GEISA 1984 and HITRAN 1996. This is largely the result of differences in the half-widths and in the temperature dependencies.

Furthermore, we investigate the temperature dependencies of the absorption coefficients. Higher temperatures lead to stronger absorption, except for regions in the far infrared. Strong temperature dependencies are found in regions with weak absorption due to the fact that in general the energy of the lower level of transition (E_l) is higher for weaker line intensities (S_l^*)

3. A Longwave Radiative Transfer Scheme for Climate Modelling and its Evaluation with Surface Observations at Cabauw

Table 3.1: Comparison of Absorption Coefficients, C_{WLA} and C_{SLA} , of Three Spectroscopic Compilations. Longwave spectral averages, weighted with the Planck function ΔB , its derivative with respect to temperature $\Delta(dB/dT)$, and wavenumber $\Delta\nu$, of the HITRAN 1996 WLA absorption coefficients (cm^2g^{-1}) and SLA absorption coefficients ($[\text{cm}^2\text{g}^{-1}]^{1/2}$) at reference temperature (250 K) and the relative differences between HITRAN 1996 and GEISA 1984 (H96-G84), between HITRAN 1996 and HITRAN 1980 (H96-H80) as well as between GEISA 1984 and HITRAN 1980 (G84-H80).

Molecule	Weighting factor	HITRAN 1996		H96-G84 (%)		H96-H80 (%)		G84-H80 (%)	
		WLA	SLA	WLA	SLA	WLA	SLA	WLA	SLA
H ₂ O	ΔB	935.	5.2	0.0	0.2	8.7	0.4	8.7	0.2
	$\Delta(dB/dT)$	460.	3.2	0.3	1.2	7.0	-1.4	6.7	-2.5
	$\Delta\nu$	749.	5.0	0.3	1.6	7.7	-1.2	7.4	-2.7
CO ₂	ΔB	138.	3.0	-3.3	-1.6	-1.0	-16.0	2.4	-14.7
	$\Delta(dB/dT)$	145.	3.0	-3.2	-1.6	-1.4	-16.0	1.8	-14.6
	$\Delta\nu$	519.	3.2	-1.3	-0.2	-7.0	-17.5	-5.8	-17.3
O ₃	ΔB	101.	10.1	0.1	11.4	7.1	8.0	6.9	-3.0
	$\Delta(dB/dT)$	148.	13.5	0.3	11.6	7.6	7.4	7.3	-3.7
	$\Delta\nu$	80.	9.1	1.0	19.7	8.2	22.8	7.2	2.6
N ₂ O	ΔB	53.	2.6	-4.3	-1.5	-4.1	-9.3	0.2	-8.0
	$\Delta(dB/dT)$	84.	3.2	-4.9	-2.0	-5.0	-10.2	-0.1	-8.4
	$\Delta\nu$	332.	5.2	-1.4	0.6	-2.9	-11.1	-1.6	-11.6
CH ₄	ΔB	40.	0.9	2.0	2.3	68.5	49.6	65.2	46.2
	$\Delta(dB/dT)$	75.	1.7	2.0	2.0	68.2	49.0	65.0	46.1
	$\Delta\nu$	72.	2.2	1.8	1.2	68.2	59.5	65.3	57.6

(see Appendix Eq.3.8). For H₂O we have found the largest temperature dependence of the WLA coefficient in the window region, mounting up to a factor 2000 for a 100 K temperature change in the 985-990 cm^{-1} spectral interval. Differences in the temperature dependencies between the spectroscopic compilations are largest in the near-infrared 4 μm region. Also, some weak lines in the window region show large differences between the HITRAN 1980 and 1996 database. On average, we find that the temperature dependency computed from the GEISA 1984 compilation is largest.

On the basis of this direct comparison, we may conclude that laboratory measurements of the spectroscopic line parameters, concerning the five most important absorbers in the longwave spectrum, converge. We find the largest difference between HITRAN 1980 and GEISA 1984, and one order of magnitude less difference between GEISA 1984 and the most recent HITRAN 1996.

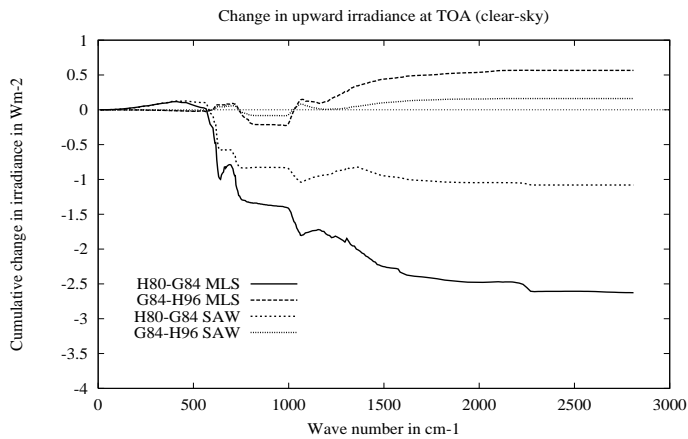
3.3 Experiments with the Narrow Band Scheme

The NBM is used to test the impact of the differences between the spectroscopic line parameters of HITRAN 1980, GEISA 1984 and HITRAN 1996. As input for the longwave radiation models we use the five clear sky reference atmospheres in which pressure, temperature, humidity and ozone mixing ratio are prescribed. The reference mixing ratio of CO₂ is 300 ppmv and considered to be uniformly mixed throughout the entire atmosphere. Additionally, the trace gases N₂O and CH₄ are set on 0.28 ppmv and 1.75 ppmv respectively and also uniformly mixed. These concentrations are chosen as to make our results comparable with ICRCM [Luther *et al.*, 1988; Ellingson *et al.*, 1991]. The middle of model's highest layer is at 45 km (2.5 hPa) in the NBM. We make a comparison of the longwave irradiances at three levels: the downward irradiance at the surface (SFC), the upward irradiance at the top of atmosphere (TOA) and the net irradiance at the tropopause (TRP). The latter is equal to the radiative heating of the surface/troposphere system. Its change due to increases of greenhouse gases or due to changes of spectroscopic data as is considered here, corresponds to the definition of (instantaneous) radiative forcing. The rationale is that these changes of adopted spectroscopic data can be translated into a temperature change at the surface (after multiplication with the model dependent climate sensitivity parameter) when applied to a representative global average atmosphere or within 3D climate models [Van Dorland *et al.*, 1997, Chapter 4]. Hence, it is a measure of the impact on the control climate.

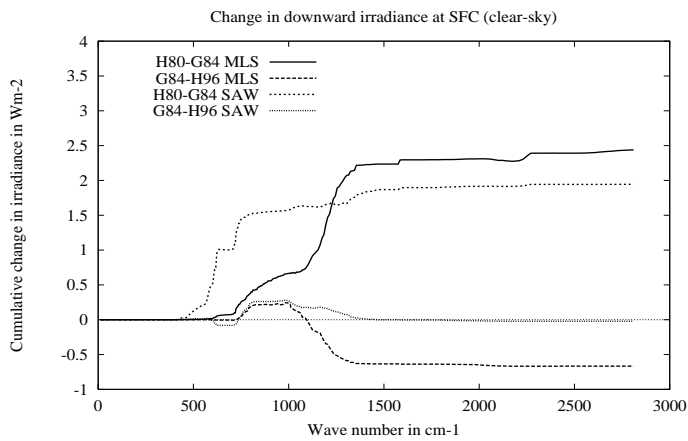
The upward irradiance at the top of atmosphere computed using the HITRAN 1980 dataset is approximately 2.6 Wm^{-2} smaller than using the GEISA 1984 compilation for the MLS atmosphere (Figure 3.1a). The HITRAN 1996 also shows a lower value of about 0.6 Wm^{-2} . This indicates that the GEISA 1984 compilation causes the most transparent atmosphere, which is also shown in Figure 3.1b and in Table 3.2 (sum-case) in which the downward longwave irradiance at the surface is 0.76 Wm^{-2} and 2.02 Wm^{-2} lower than using the HITRAN 1996 and 1980 data, respectively. Differences between the two oldest compilations are considerably larger than between HITRAN 1996 and GEISA 1984. We find the same features in the Sub-Arctic Winter (SAW) atmosphere, but differences are reduced by a factor 2 to 3 due to the fact that the surface temperature is much lower, resulting in a strong reduction of the upward longwave irradiance and therefore of the absorbed radiation by greenhouse gases and also because the SAW atmosphere contains considerably less water vapour.

In order to investigate the origin of the differences between the GEISA 1984 and the HITRAN 1996 compilations, we consider the spectral cumulative changes in net irradiance at the tropopause (radiative forcing) for the individual gases. Thereto, computations are performed using a reference atmosphere with the HITRAN 1996 data and replacing the spectroscopic parameters for each gas with the GEISA 1984 values separately (Figure 3.2). In the MLS atmosphere, the total difference of 0.5 Wm^{-2} is entirely caused by water vapour as the differences in radiative effects of the remaining four greenhouse gases cancel each other quite well. The spectroscopic data change from HITRAN 1996 to GEISA 1984 results in a positive radiative forcing for water

3. A Longwave Radiative Transfer Scheme for Climate Modelling and its Evaluation with Surface Observations at Cabauw



(a)



(b)

Figure 3.1: (a) Cumulative change in upward irradiance (in Wm^{-2}) at the top of atmosphere (TOA) under clear sky conditions for the Mid-Latitude Summer (MLS) as well as the Sub-Arctic Winter (SAW) atmosphere due differences in processed spectroscopic data, between HITRAN 1980 and GEISA 1984 (H80-G84) and between GEISA 1984 and HITRAN 1996 (G84-H96). (b) Same as 1a, but for the (absolute value of) downward irradiance at the surface (SFC).

vapour lines in the region 0 to 1100 cm^{-1} and a much larger negative forcing in the remaining part of the longwave spectrum. For CO_2 , the P-branch (rotational lines in the longwave wing) of the strong 15 μm band shows a negative radiative forcing, while in the R-branch (shortwave wing) the opposite is true. For ozone, we find the largest changes in radiative forcing in the

Table 3.2: NBM downward longwave irradiance (Wm^{-2}) at the surface (SFC) and at the tropopause (TRP) in the Mid-Latitude Summer atmosphere under clear sky conditions using different spectroscopic data for the individual greenhouse gases (H80=HITRAN 1980, G84=GEISA 1984, and H96=HITRAN 1996). The total counterirradiation (all) including the effects of CFCs (0.82 Wm^{-2} at SFC and 0.06 Wm^{-2} at TRP) and the water vapour continuum (232.50 Wm^{-2} at SFC and 0.04 Wm^{-2} at TRP) following Giorgetta and Wild [1995] is also tabulated.

Component	F ⁻ (SFC)			F ⁻ (TRP)		
	H80	G84	H96	H80	G84	H96
Line spectra						
H ₂ O (MLS-profile)	259.03	254.37	255.67	6.66	6.97	6.97
CO ₂ (300 ppmv)	78.24	74.82	74.38	12.20	11.06	11.08
O ₃ (MLS-profile)	6.38	6.43	6.49	3.40	3.26	3.33
N ₂ O (280 ppbv)	7.60	7.40	7.17	0.46	0.45	0.44
CH ₄ (1750 ppbv)	5.47	6.92	7.46	0.17	0.24	0.24
Combinations						
All (including CFCs)	356.03	354.01	354.77	22.22	21.39	21.48
H ₂ O+CO ₂ +O ₃	354.17	351.07	351.99	21.60	20.71	20.80
H ₂ O+CO ₂	351.29	348.12	349.00	18.89	18.06	18.07
H ₂ O (lines+continuum)	348.67	345.81	346.76	6.71	7.02	7.01

vicinity of the strong $9.6 \mu\text{m}$ band as the result of the addition of weaker lines and new half-width measurements including its temperature dependencies (section 3.2.3). The changes in the N₂O 7.8 and $8.6 \mu\text{m}$ bands and in the CH₄ $7.7 \mu\text{m}$ band cancel each other to a large extent. We find differences in net irradiance at the tropopause up to 5 Wm^{-2} between HITRAN 1980 and GEISA 1984 for the tropical atmosphere in which the three most important greenhouse gases (H₂O, CO₂ and O₃) are included. This difference is larger than for an atmosphere in which all gases are incorporated due to the fact that the lack of CH₄ data in HITRAN 1980 makes the atmosphere less opaque. Although this change in spectroscopic data affects the radiation balance considerably (5 Wm^{-2} corresponds to a change of about 1.7% of the total net irradiance at the tropopause), the relative changes in sensitivity to increases of CO₂ are of the same order, hence not very significant for climate perturbation studies.

Furthermore, a comparison has been made for the downward irradiance at the surface as well as at the tropopause due to the individual species (H₂O with and without continuum, CO₂, O₃, N₂O and CH₄) between the three investigated spectroscopic datasets in the MLS atmosphere (Table 3.2). Water vapour is the main contributor (about 77%) to the downward irradiance at the surface due to the fact that H₂O has a very high mixing ratio in the lower troposphere relative to the other radiatively active gases, while its absorption coefficients are rather strong (Table 3.1). In contrast, CO₂ is contributing most to the counter-radiation at the tropopause, about 51% in the GEISA 1984 and HITRAN 1996 cases and about 54% in the HITRAN 1980 case, due

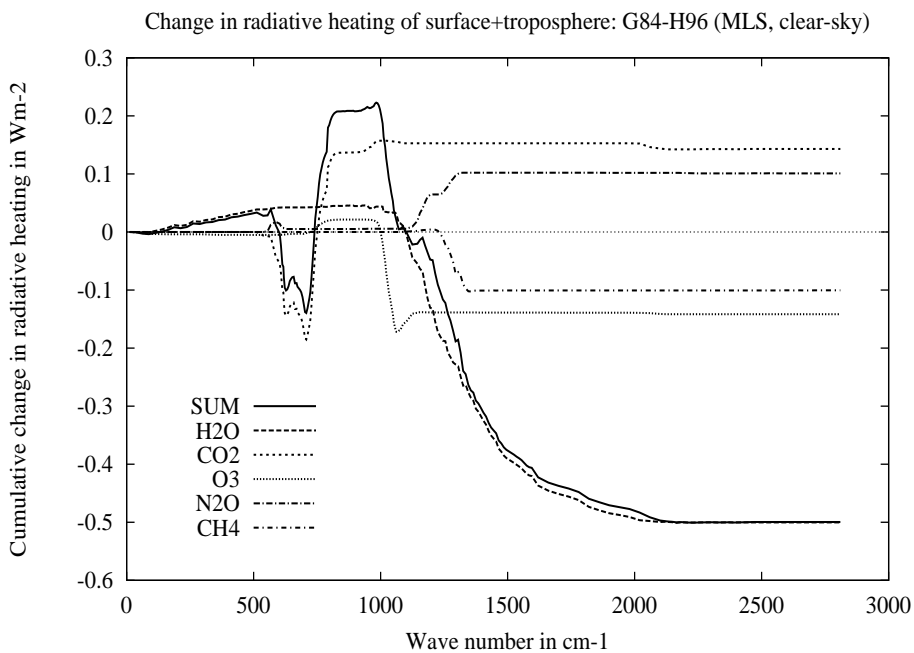
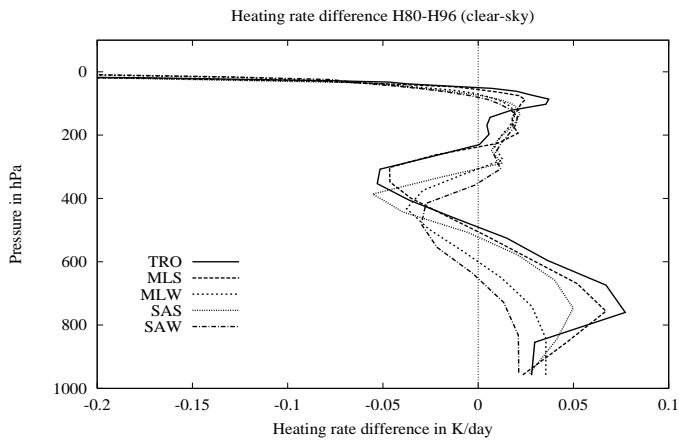


Figure 3.2: Cumulative change in radiative heating of the surface/troposphere system (i.e. net downward irradiance at the tropopause) for the MLS atmosphere due to differences in spectroscopic data between GEISA 1984 and HITRAN 1996 of the investigated greenhouse gases and their sum.

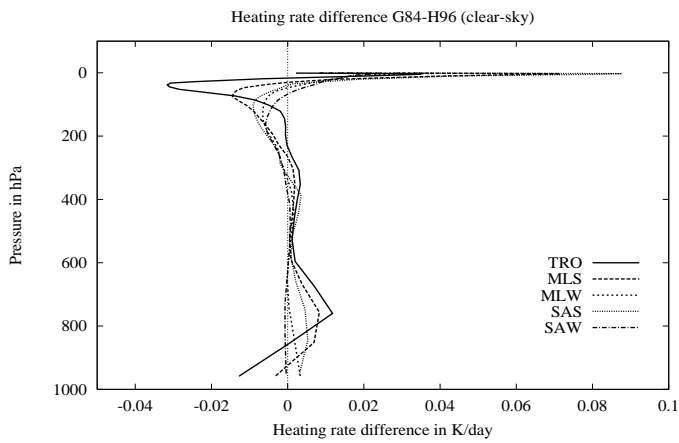
to the higher mean SLA absorption coefficient of CO_2 in the oldest compilation. Downward irradiances from the individual species at the tropopause can be added within a few percent accuracy due to the small absorber amounts in the stratosphere, while at the surface the overlap effect causes a smaller total downward irradiance than the sum of the irradiances, computed for the individual absorbers. The differences in downward irradiances at the tropopause due to N_2O and CH_4 are also reflecting the differences in (mean) absorption coefficients listed in Table 3.1. Since increases of these greenhouse gases show a square root dependence [Cess *et al.*, 1986; Ramanathan *et al.*, 1987; IPCC, 1990], both absorption coefficients, WLA and SLA, determine the optical thickness. In contrast, for H_2O and CO_2 there is a logarithmic dependence, indicating the SLA regime for these absorbers.

Heating rates computed with the HITRAN 1980 data for the five reference atmospheres show less cooling in the lower part of the troposphere (and in the lower part of stratosphere) as compared to GEISA 1984 (Figure 3.3a). In the upper troposphere the situation is reversed. The differences in the troposphere are in good agreement with the radiative effects of larger absorption coefficients of CO_2 and to a lesser extent of H_2O in the HITRAN 1980 compilation. The differences in heating rate between the HITRAN 1996 and the GEISA 1984 spectroscopic data are

3. A Longwave Radiative Transfer Scheme for Climate Modelling and its Evaluation with Surface Observations at Cabauw



(a)



(b)

Figure 3.3: Differences in heating rate (K/day) for five reference atmospheres due to changes in spectroscopic data, using the NBM: (a) HITRAN 1980 - HITRAN 1996 and (b) GEISA 1984 - HITRAN 1996.

an order of magnitude smaller (Figure 3.3b, mind the different scales). This is also in agreement with our findings of the direct comparison of the spectroscopic compilations (section 3.2.3). Also, we conclude that using the GEISA 1984 spectroscopic line parameters, the atmosphere is more transparent as compared to both HITRAN compilations.

3.4 The Wide Band Radiation Scheme

3.4.1 Transmissivity Parameterizations

The longwave WBM uses a broad band flux emissivity method with six intervals covering the spectrum between 0 and 2820 cm^{-1} (Table 3.3) and has been derived from the ECMWF radiation code [Morcrette, 1989; 1991]. The original code contains H_2O absorption in all intervals, e- and p-type continuum absorption [Roberts *et al.*, 1976] between 350 and 1250 cm^{-1} , CO_2 absorption and O_3 absorption between 970 and 1110 cm^{-1} . It also accounts for (linear) aerosol absorption. Cloud effects are included in terms of cloud droplet absorption computed from the liquid water path using an emissivity formulation. Scattering by clouds is neglected in the longwave spectrum. We add CH_4 , N_2O , and 16 CFCs, HCFCs and HFCs to the radiation scheme for climate modelling purposes. Also, we include the $14\text{ }\mu\text{m}$ band of ozone, since this band contributes significantly to atmospheric radiative transfer [Shine *et al.*, 1995]. Here we replace the longwave (and optical) parameters of five types of aerosols [Tanné *et al.*, 1984] by those of 11 aerosol components of the Global Aerosol Data Set [d'Almeida *et al.*, 1991; Koepke *et al.*, 1997]. A major update concerns the formulation of the water vapour continuum, which is based on Ma and Tipping [1992] and further described in Giorgetta and Wild [1995]. Overlap of the various absorbers in each of the six spectral bands is computed using multiplication of their transmissivities. We utilize the reference version of our WBM with the parameterized spectroscopic line parameters of the most recent HITRAN 1996.

In the WBM, Eqs.3.2 and 3.3 are evaluated numerically after discretization over the vertical grid and with respect to the six spectral intervals. The band averaged irradiances are evaluated with the help of band-transmissivities pre-calculated from the NBM of Morcrette and Fouquart [1985]. The formulation accounts for different temperature dependencies involved in atmospheric radiative transfer. Firstly, the temperature T_p at the level where irradiances are calculated. Secondly, the average temperature, T_u , along the absorption path between two pressure levels (p and p'), which determines the transmission via the temperature dependence of the intensities and half-widths of the lines in the broad spectral bands. The band transmissivities are calculated non-isothermally, accounting for the temperature dependence that arises from the product of the monochromatic transmission and the Planck function. Therefore, two normalized band transmissivities are used for each absorber in the considered spectral regions, namely one scaled with the Planck function for the computation of the transmission of the radiation originating from the boundaries (first terms on the r.h.s. of Eqs.3.2 and 3.3) and one scaled with the temperature derivative of the Planck function to evaluate the integrals (last terms on the r.h.s. of Eqs.3.2 and 3.3). Although the actual dependence on T_p is carried out explicitly in the Planck functions integrated over the spectral regions, the transmissivities still depend on T_u , both through Wien's displacement law and through the temperature dependence of the spectroscopic parameters.

For the gases H_2O , CO_2 , N_2O and CH_4 , the transmissivities have been expanded into Padé

Table 3.3: Characteristics of the WBM: spectral intervals and the corresponding band contours of the most important greenhouse gases. The ratio of the coefficients for the (p-e)-type and e-type water vapour continuum absorption (γ_n) between 350 cm^{-1} and 1250 cm^{-1} is also listed.

Spectral region (cm^{-1})	Band contours	Continuum (γ_n)
0-350 & 1450-1880	rotation and vibration-rotation bands of H ₂ O	
500-800	15 μm band of CO ₂	0.017
800-970 & 1110-1250	atmospheric window, 8.6 and 10.7 μm bands of N ₂ O, and wings of 7.7 μm band of CH ₄	0.0025
970-1110	9.6 μm band of O ₃	0.0018
350-500	25 μm window region of H ₂ O	0.059
1250-1450 & 1880-2820	7.8 μm band of N ₂ O and 7.7 μm band of CH ₄	

approximants [Brezinski, 1985]:

$$\tau(T_u, \overline{u\overline{p}}) = \sum_{i=0}^2 F_i (u_e p_e)^{i/2} / \sum_{j=0}^2 G_j (u_e p_e)^{j/2} \quad (3.6)$$

where $u_e p_e = r \cdot \overline{u\overline{p}} \cdot f(T_u, \overline{u\overline{p}})$ is an effective amount of absorber which incorporates the diffusivity factor r , the pressure scaling of the absorber amount $\overline{u\overline{p}}$, and the temperature dependence of the absorption coefficients, given by:

$$f(T_u, \overline{u\overline{p}}) = \exp[a(\overline{u\overline{p}})(T_u - T_0) + b(\overline{u\overline{p}})(T_u - T_0)^2] \quad (3.7)$$

where $a(\overline{u\overline{p}})$ and $b(\overline{u\overline{p}})$ are second order polynomials with respect to $\log(\overline{u\overline{p}})$, derived from the best fit using NBM calculations and T_0 is a reference temperature (here $T_0=250 \text{ K}$). In fact, we use in Eq.3.7 a similar functional relationship as the temperature dependencies of the SLA coefficient for the NBM spectral intervals, following *Rodgers and Walshaw* [1966] (see Appendix, Eq.3.17). The temperature dependence due to Wien's law is incorporated by the pre-calculated coefficients F_i and G_j for temperatures between 187.5 K and 312.5 K in steps of 12.5 K. This Padé approximation is chosen for computational efficiency and for its suitability for representing the three absorption regimes, namely linear for weak absorption, square root for intermediate absorption and logarithmic for strong absorption.

For the transmissivity of ozone in the 9.6 μm region a two-path version of the Malkmus random band model is used [Rodgers, 1968]. The 14 μm band of O₃ is parameterized in terms of the single-path version of the Malkmus model (Appendix, Eq.3.10). The band averaged absorption coefficients of the 16 CFCs, HCFCs and HFCs are directly computed from the band absorptances given in the AFEAS [1989] report. The strong line intensities, resulting in weak temperature dependencies (see Appendix), in combination with the rather small absorber amounts leads to a small optical thickness and thus in the weak absorption regime. The water vapour continuum formulation is taken from *Ma and Tipping* [1992] and calculated for the six intervals

[Giorgetta and Wild, 1995]. The ratio between the (p-e)-type and the e-type strength (γ_n) for the four of the six spectral intervals is listed in Table 3.3. Sensitivity tests using the reference atmospheres show differences of 10 to 13 Wm^{-2} in downward longwave radiation at the surface as compared to the continuum by Roberts *et al.* [1976]. Therefore, uncertainties due to the water vapour continuum formulation in radiative transfer schemes are quite large as compared to uncertainties in spectroscopic line parameters.

3.4.2 Comparison with the Narrow Band Scheme

In order to compare the Wide Band Scheme with the Narrow Band Scheme, we perform radiation computations using the five reference atmospheres. To avoid numerical discrepancies, we use the same vertical integration algorithm as well as the same vertical resolution (27 layers) in both schemes. Furthermore, we use the HITRAN 1996 spectroscopic data, evaluated with the help of statistical band models for the NBM and further parameterized towards the six spectral bands in the WBM following the method described in section 3.4.1. In Figure 3.4a, the heating rates computed with the NBM are shown. In general, the longwave tendencies act to cool the atmosphere due to the fact that emission dominates the absorption to a large extent. In the troposphere, the heating rates are of the order of -1 to -2 K/day, depending on temperature and water vapour content. In the tropical atmosphere, we find a slight warming around the 100 hPa pressure level. The differences between WBM and NBM are of the order of 0.05 K/day, which is about 5% of the typical heating rates in the troposphere (Figure 3.4b), while atmospheric averages are smaller than 0.02 K/day. These errors are of the same order as the differences between the heating rates computed with the NBM using the HITRAN 1980 and the HITRAN 1996 spectroscopic datasets (see Figure 3.3). Since we find that differences between the most recent spectroscopic line parameters are considerably less, we may conclude that improvement of radiation codes can be accomplished by increasing the spectral resolution rather than the implementation of newer spectroscopic data.

3.5 Evaluation of the Wide Band Scheme at the Surface

3.5.1 Cabauw Observations and Data Quality

The ultimate test for radiation schemes is the comparison with radiation measurements, which are performed on routine basis from satellites and ground based networks. Typically, satellites measure outgoing radiation at the top of the atmosphere in several channels. These radiances have to be processed into irradiances by performing angle integrations under assumption of a certain angular distribution. For longwave radiation, this translation is quite straightforward by virtue of the approximate isotropic behaviour. Surface radiation is typically measured in broad bands, i.e. the entire longwave spectrum or in the window region. On average, the upward and downward longwave irradiances are the largest components of the energy exchange between the

3. A Longwave Radiative Transfer Scheme for Climate Modelling and its Evaluation with Surface Observations at Cabauw

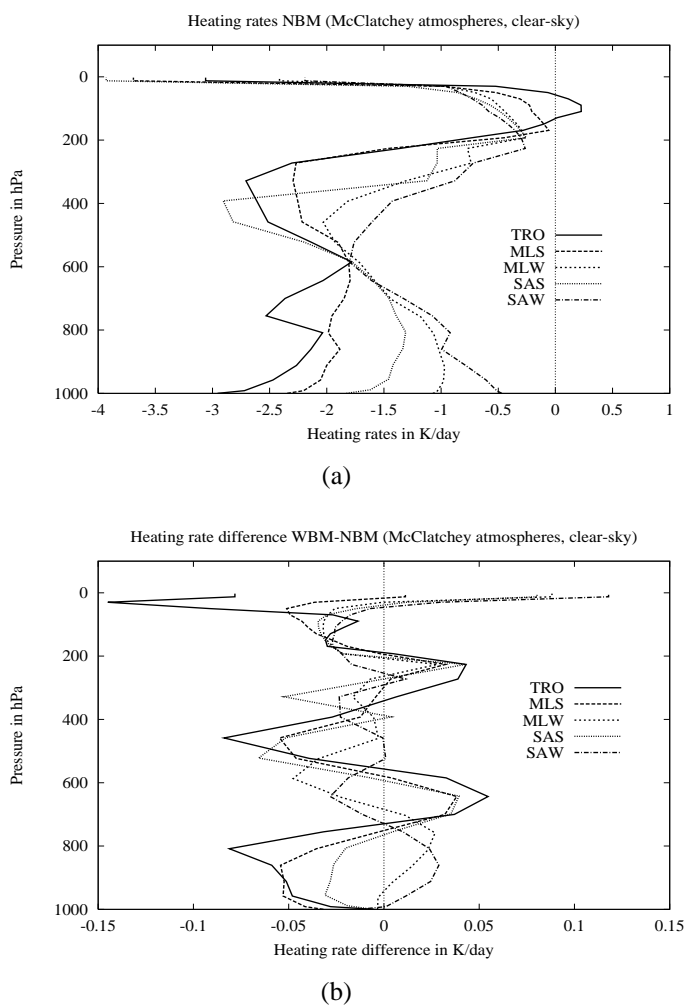


Figure 3.4: Heating rate computed with the Narrow Band Model (a) and difference in heating rate in K/day between the Wide Band Model and the Narrow Band Model (b) using the HITRAN 1996 spectroscopic data, tested for the five reference profiles.

atmosphere and the surface. The upward radiation can be computed with Stefan-Boltzmann's law, which is only dependent on surface temperature, since the surface can be considered as a black body. The downward component of the longwave radiation at the surface originates from the atmosphere due to thermal emission by greenhouse gases, clouds and aerosols. Accurate modelling of the atmospheric counter-radiation is crucial, since it affects directly the surface energy balance. Most GCMs underestimate this incoming longwave radiation [Wild *et al.*, 1995].

Here we evaluate the radiation scheme with the downward longwave radiation, measured under clear sky conditions at the Cabauw site (station 06348 at 51°58'N, 04°56'E). Clouds increase the downward longwave emission as compared to the thermal emission by greenhouse gases, mainly in the atmospheric window region. This increase depends on the cloud fraction and cloud temperature. Moreover, the incorporation of cloud effects on radiative transfer necessitates an accurate knowledge of the cloud parameters such as cloud base altitude, vertical extent and overlap in case of multi-level clouds.

We select clear sky 'hours', coinciding with the times of the rawind sonde measurements every six hours according to the WMO standards, in the period 1995-1996. During these years ten stations distributed over a 120×120 km area in the vicinity of the Cabauw site were equipped with cloud detection as well as radiation instruments for the TEBEX campaign [Van Lammeren *et al.*, 1998]. At the Cabauw site we use the Eppley pyrgeometer (PIR) for the comparison with our modelled downward longwave radiation at the surface. In the first eight months of the TEBEX campaign, which started in January 1995, the quality of the pyrgeometer data was insufficient. In the remaining period about 2000 hours are subjected to an investigation on clear sky conditions. These conditions are checked using radiation measurements in the TEBEX area. Doubtful situations are further checked with NOAA satellite images on the presence of (high) clouds. Finally, we have 253 hours for our comparison under clear skies.

Concerning the radiation measurements, we discern two types of error sources: instrumental errors and exposure errors. Instrumental errors can be divided in calibration errors and errors in measuring the signals of the instrument. The Eppley pyrgeometer we used has three output signals: one for the thermopile, one for the thermistor sensing the temperature of the housing and one for the thermistor sensing the temperature of the dome that acts as an optical filter. This pyrgeometer was calibrated by the World Radiation Centre in Davos, Switzerland, following a procedure as described by Philipona *et al.* [1995] and Kohsiek and Van Lammeren [1997]. Although the relative accuracy of the calibration is better than 1 Wm^{-2} , the absolute accuracy is not better than a few Wm^{-2} , mainly because of lack of a world-wide accepted standard procedure for calibration [Philipona *et al.*, 1998].

Errors may further be introduced by the whole electronical chain from sensor to data output. In this case, inaccuracies in the electronics for the thermistor signals contribute most. For instance, an error of 0.1 K in the temperature difference between housing and dome is quite possible, and this introduces an error of about 2 Wm^{-2} . Exposure errors can be occasioned by obstacles, which were virtually absent in our situation, and by sunshine heating the dome in a non-uniform way. The latter situation was taken care of by actually measuring the dome temperature by four thermistors which were electrically interconnected. Taking all into account, we estimate that there may be a systematic error of 2 Wm^{-2} due to the calibration, and a random error of 5 Wm^{-2} due to other causes.

Table 3.4: Sensitivity due to uncertainties in atmospheric conditions, as tested for the 253 atmospheric cases at Cabauw (LWP=liquid water path and IWP=ice water path).

Variable	Variation	Sensitivity in Wm^{-2}
Temperature	+0.2 K (profile)	+0.64
Humidity	+10% (profile)	+2.40
Ozone (constant total column)	+50% O_3 (troposphere)	+0.75
Aerosols (water soluble)	+0.1 optical thickness	+0.25
Cirrus (IWP=0.1 gm^{-2})	+1 octa	+0.06
Cirrus (IWP=1.0 gm^{-2})	+1 octa	+0.55
Low clouds (LWP=0.1 gm^{-2})	+1 octa	+0.21

3.5.2 Model Inputs and Sensitivity

Observations of the profiles of temperature and humidity, gathered at the 200 m tower at Cabauw, are used as input for the WBM in order to model the atmospheric conditions as well as possible. Hourly averaged tower profiles are combined with profiles higher up in the atmosphere (200 m to approximately 30 km), measured by the rawind sonde at De Bilt, which is situated within a distance of 30 km from Cabauw. In case of gaps in the Cabauw profiles, we use rawind sonde data. For instance, for temperatures below the freezing point no accurate humidity data are available from the Cabauw tower. We use the ozone vertical profile of the Mid-Latitude Summer reference atmosphere scaled with the total column ozone measurements derived from the Brewer spectrophotometer at De Bilt. For the concentrations of the uniformly mixed gases, such as CO_2 , CH_4 etc., we adopt the 1995 values of IPCC [1995].

We perform several model computations to determine the impact of possible (systematic) errors in the measurements of the atmospheric profiles used for the computations of the downward irradiance at the surface. For instance, if we add 0.2 K to the measured temperature profile, we find an increase of the downward longwave irradiance of about 0.64 Wm^{-2} (see Table 3.4). Also, increasing the mixing ratio of water vapour by 10% in the troposphere causes a rather large impact on the computed counterradiation, namely 2.4 Wm^{-2} . Since we use the ozone profile of the MLS atmosphere scaled with the measured total ozone column value, we may make errors in the ozone distribution. Adopting 50% more ozone in the troposphere, while removing the same amount proportionally from the stratosphere, cause an additional counterradiation of 0.75 Wm^{-2} . This could be the case for highly polluted (smog) days, which may happen more often under clear sky conditions [Lelieveld and Van Dorland, 1995; Fortuin et al., 1995b]. The same holds for the incorporation of water soluble aerosols, which are mainly active in the shortwave spectrum, but also possess absorption properties in the infrared, resulting in more counterradiation. It is also possible that we have overseen some (subvisual) high clouds as our clear sky detection algorithm is unable to detect such clouds. In case of total coverage of cirrus with an

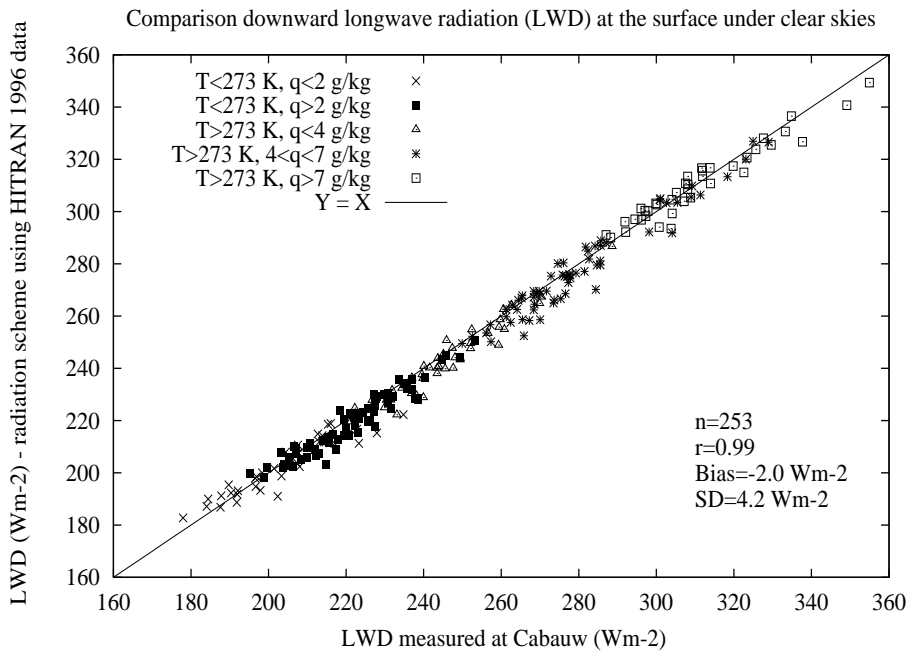


Figure 3.5: Comparison of downward longwave radiation computed with the radiative transfer scheme using parameterized HITRAN 1996 data and Cabauw measurements under clear sky conditions.

ice water path of 0.1 gm⁻², the downward irradiance will increase with 0.5 Wm⁻². Adding up quadratically all uncertainties, we find an uncertainty in the model results due to possible errors in the input parameters of about 3 Wm⁻². Although errors in the temperature, humidity and ozone profiles may be considered as random, giving rise to some amount of scatter in the comparison between model calculations and measurements, the omission of aerosols and overseen clouds may bias the result in terms of computing on average less counter-radiation than measured.

3.5.3 Comparison of the Wide Band Scheme with Observations

The comparison between the downward longwave irradiance measurements at the surface at Cabauw and the calculations by the radiation scheme (WBM) is shown in Figure 3.5. For a large range of temperatures and humidities, resulting in downward radiative fluxes between 180 and 360 Wm⁻², the WBM using the HITRAN 1996 data performs well. The mean difference (bias) between model and measurements is only -2.0 Wm⁻², while the standard deviation of 4.2 Wm⁻² is of the same order as the radiation measurement errors (see section 3.5.1) and possible errors related to the measured atmospheric profiles used as input for the WBM (see

section 3.5.2). The negative bias of -2 Wm^{-2} agrees with our expectation that on average we model less counterradiation than measured. Moreover, this bias is of the same order as the estimated systematic error in radiation measurements (see section 3.5.1). No systematic errors are found when the 253 cases are split into five classes of temperature and humidity regimes (Figure 3.5).

The setup of the comparison between the radiation measurements and the computations with the longwave radiative transfer scheme facilitates the test of spectroscopic databases and the water vapour continuum formulation, which is parameterized separately in our NBM and WBM. Here, we also consider the radiative transfer scheme of the ECHAM4 climate model [Roeckner *et al.*, 1996], in which a combination of the investigated spectroscopic datasets is implemented. Except for this difference, the ECHAM4 radiation scheme is identical to our WBM. Line spectra of H_2O , CO_2 and N_2O are taken from HITRAN 1980, while the temperature dependencies of their broad band absorption as well as emission are slightly modified (M. Giorgetta, priv. comm.). For O_3 , absorption properties are taken from the GEISA 1984 database, while for CH_4 , the HITRAN 1991 dataset is used, which agrees quite well with the HITRAN 1996 spectroscopic data (not shown in this paper). Due to the fact that H_2O and CO_2 are by far the most important greenhouse gases, especially if we consider the counterradiation at the surface, the replacement of the ECHAM4 "mix" by the parameterized HITRAN 1980 data shows the smallest average difference of downward longwave irradiance for the investigated 253 cases, namely 2.6 Wm^{-2} (Table 3.5). As can be expected from our NBM experiments, the GEISA 1984 spectroscopic data results in the lowest downward irradiance. The replacement of the ECHAM4 continuum by the ECMWF continuum (until 1997 used) [Morcrette, 1989], results in a large decrease of counterradiation by 12.5 Wm^{-2} . The bias of -11.1 Wm^{-2} is unrealistically large as compared to the assumed accuracy of the radiation measurements. Therefore, we can conclude that the old continuum formulation is not correct. The sensitivities to doubling the CO_2 as well as the CH_4 content of the atmosphere is also shown in Table 3.5, resulting in an increase of longwave radiation at the surface of 1.7 Wm^{-2} and 0.7 Wm^{-2} , respectively. From this point, it will be clear that, considering the uncertainty in radiation measurements, increases of greenhouse gases can hardly be detected from increases of counterradiation at the surface.

3.6 Summary and Conclusions

In this study, we develop a wide band longwave radiative transfer scheme (WBM), which is sufficiently computationally efficient to be used in 3D climate models (e.g. ECHAM4). In this WBM we include the most important absorption bands of greenhouse gases, necessary to study climate change, e.g. due to activities of mankind in the last century. In order to test the performance of our WBM, we compare the heating rates with those computed with the Narrow Band Model (NBM) using the five reference profiles [McClatchey *et al.*, 1972], covering a wide range of atmospheric conditions. Furthermore, the same profiles are used to study the impact of spec-

Table 3.5: Bias and standard deviation (SD) in Wm^{-2} as compared to the downward irradiance measurements for the 253 cases at Cabauw. The old continuum refers to ECMWF continuum until 1997 [Morcrette, 1989].

Spectroscopic data	Bias in Wm^{-2}	SD in Wm^{-2}
HITRAN 1996	-2.0	4.2
GEISA 1984	-2.4	4.2
HITRAN 1980	-1.2	4.2
ECHAM4 "mix"	1.5	4.4
ECHAM4 with old continuum	-11.1	4.6
Perturbation experiment		
HITRAN 1996: $2 \times \text{CO}_2$	-0.3	4.3
HITRAN 1996: $2 \times \text{CH}_4$	-1.3	4.2

troscopic line parameters, which form the basis of radiation computations. Finally, we compare the WBM downward irradiance at the surface with radiation measurements at the Cabauw site in the Netherlands as an ultimate test of the radiation scheme.

Concerning the differences between spectroscopic line parameters, we perform a direct comparison by averaging these parameters over the entire longwave spectrum using the Planck function and its derivative with respect to temperature as a weight function. Also, we perform radiation computations with the NBM model using the reference atmospheres as a testbed, in order to weight the direct differences with the abundance of greenhouse gases in the real atmosphere as well as to take the typical thermal structure into account. Both methods show that using the GEISA 1984 line parameters result in the most transparent atmosphere, implying least absorption as well as emission by the incorporated greenhouse gases. Furthermore, we find that differences between the oldest two compilations, HITRAN 1980 and GEISA 1984, are about one order of magnitude larger than between GEISA 1984 and HITRAN 1996. This suggests that laboratory measurements of the spectroscopic characteristics of the investigated gases are converging. This conclusion is in agreement with recent findings [Pinnock and Shine, 1998].

There are several ways to interpret differences between spectroscopic compilations. Firstly, the difference in heating rate, which is an important measure of radiative effects in 3D climate as well as weather models. Differences between HITRAN 1996 and HITRAN 1980 are of the order 0.1 K/day, while differences between the former and GEISA 1984 are of the order of 0.01 K/day. Irradiances at the boundaries, i.e. the surface and the top of the atmosphere, are important for climate modelling, since they determine the (long-term) budgets. We find differences between HITRAN 1996 and HITRAN 1980 (GEISA 1984) of the order of 2 Wm^{-2} (0.5 Wm^{-2}). The largest differences occur for the warm humid atmospheres. Comparing the same spectroscopic datasets as mentioned above, we find differences in terms of net irradiance at the tropopause of 5 Wm^{-2}

and 0.5 Wm^{-2} , respectively.

The parameterization of the transmissivities, including the temperature and pressure dependencies, of each individual greenhouse gas for the WBM, introduces heating rate errors of the order of 0.05 K/day as compared to the NBM, used as a benchmark here. Comparing the irradiances at the surface as well as the top of atmosphere between the NBM and WBM, we find differences of the order of $1\text{-}3 \text{ Wm}^{-2}$.

In this study, we evaluate the WBM with surface radiation measurements at Cabauw (The Netherlands). Thereto, we equipped the WBM with the parameterizations of the most recent spectroscopic compilation, namely HITRAN 1996. We select 253 clear-sky hours during the TEBEX period (1995-1996). Observations of temperature, humidity and ozone are combined and used as input for the WBM. Averaged over a large range of measured counterradiation at the surface, namely between 180 and 360 Wm^{-2} , the WBM computes only 2 Wm^{-2} less than observed. We find a standard deviation of 4.2 Wm^{-2} , which is of the same order as the random errors of the radiation measurements and the uncertainties in the specification of the adopted atmospheric profiles. The negative bias agrees with the idea of the omission of aerosols and overseen (subvisual) cirrus clouds in the WBM computations, which can only enhance the downward component of the longwave radiation at the surface. Using the ECHAM4 mix of spectroscopic data, the WBM has a positive bias of 1.5 Wm^{-2} as compared to the measurements. In absolute sense, this is a better result. However, it contradicts our expectation that the bias should have a small negative value.

We also investigate the impact of two formulations of the water vapour continuum, namely the formulation of *Roberts et al.* [1976], and the one based on *Ma and Tipping* [1992] and further described by *Giorgetta and Wild* [1995]. The latter formulation is used in our reference version of the WBM together with the HITRAN 1996 data. Using the 253 cases, described above, we find that the former formulation results in 12.5 Wm^{-2} less counterradiation as compared to the reference formulation. Its impact is much larger than the differences between the spectroscopic datasets and also than the magnitude of the parameterization errors from NBM to WBM. Moreover, since the large negative bias lies outside the range of the estimated uncertainties in the radiation measurements, we may reject this continuum formulation.

Concludingly, improvement of atmospheric radiative transfer in climate models can be accomplished by increasing the spectral resolution in WBMs, rather than further improvement of laboratory measurements of spectroscopic line parameters. The efforts by the spectroscopists to measure the characteristics of the enormous amounts of lines, apparently resulted in a high quality data set, which in parameterized form for the WBM compares well with observations. Also, we recommend further validation of the water vapour continuum and its dependencies on temperature and possibly pressure with in situ measurements, preferably with high resolution spectral instruments.

Acknowledgements

The authors wish to thank J.-J. Morcrette for making available the basic versions of the Narrow Band as well as the Wide Band schemes. We acknowledge N. Husson and L.S. Rothman for kindly providing us the GEISA 1984 and the HITRAN 1996 versions of spectroscopic line data, respectively; A. van Lammeren, A. Feijt, J. Konings and F. Bosveld for their help with the TEBEX data and rawind sonde profiles during the TEBEX period; the SINDICATE group and in particular E. Roeckner for their keen interest and the valuable discussions. Part of this study has been carried out within the framework of the SINDICATE project, supported by the Environmental Program of the European Union (DG-XII).

3.A Appendix: Processing Spectroscopic Line Parameters

3.A.1 Temperature and Pressure Dependencies

We use the following spectroscopic parameters in order to process them into random band model parameters for the NBM: wavenumber of the absorption line ν_l (cm^{-1}), line intensity S_l^* (cm molecule^{-1}) at 296 K, collision half-width α_l^* ($\text{cm}^{-1}\text{atm}^{-1}$) at 296 K, energy of the lower level of transition E_l (cm^{-1}) and temperature dependence coefficient n of α_l^* .

Infrared absorption and emission is strongly dependent on temperature T and pressure p along the absorption path, because S_l^* is a function of T and α_l^* is a function of T as well as p . The temperature dependence of S_l^* , which is in general strong for weak lines due to large values of E_l , can be derived from quantum mechanics [Smith *et al.*, 1985]:

$$S_l^*(T) = S_l^*(T_s) \frac{1 - \exp[-c_2\nu_l/T]}{1 - \exp[-c_2\nu_l/T_s]} \frac{Q(T_s)}{Q(T)} \exp[c_2E_l(\frac{1}{T_s} - \frac{1}{T})] \quad (3.8)$$

where $c_2 = h.c/k_B = 1.439$ cm K, $T_s = 296$ K, $Q(T) = Q_v(T) \cdot Q_r(T)$ is the total partition function, $Q_v(T)$ is the vibrational partition function and $Q_r(T) = (T/T_s)^j$ is the rotational partition function (values of Q_v and j are listed in Table 3.6).

The temperature and pressure dependence of the half-widths, caused by collision broadening, and resulting in a Lorentzian line shape can be written as:

$$\alpha_l(T, p) = \alpha_l(T_s, p_0) \frac{p}{p_0} \left(\frac{T_s}{T}\right)^n \quad (3.9)$$

where p_0 is the reference pressure (1 atm) and n is given in the GEISA 1984 [Chedin *et al.*, 1986] and HITRAN 1996 compilations; where no measurement is given, i.e. in HITRAN 1980 and occasionally in GEISA 1984, we have taken the values used by Morcrette [1984] ($n = 0.62$ for H_2O and $n = 0.50$ for CO_2 , O_3 , N_2O and CH_4). Note that α_l^* , given in the compilations, can be written as $\alpha_l(T_s, p_0)/p_0$.

3.A.2 Random Band Models

In the Narrow Band Model, the longwave spectrum between 0 and 2820 cm^{-1} is divided into 225 narrow bands. The widths of the spectral intervals, ranging from 2 to 40 cm^{-1} , have been chosen according to the absorption properties of the various absorbers included in the model. The transmission functions for each spectral interval are computed with the help of two statistical band models. The choice of the model depends on the distribution of the line intensities within the narrow intervals. For H_2O , CO_2 and O_3 the Malkmus model is used:

$$\tau(p, p') = \exp\left[-\frac{B_0 u_e p_e}{2u_e} \left(\sqrt{1 + 4 \frac{A_0 u_e^2}{B_0 u_e p_e}} - 1\right)\right] \quad (3.10)$$

while for N₂O and CH₄ the Goody model is used:

$$\tau(p, p') = \exp\left[-A_0 u_e / \sqrt{1 + \frac{A_0 u_e^2}{B_0 u_e p_e}}\right] \quad (3.11)$$

where $\tau(p, p')$ is the transmissivity between pressure level p and p' , A_0 is the ratio of mean line intensity and mean line distance at 250 K (see Eq.3.12), B_0 is the line structure parameter, i.e. ratio of weighted half-width (with line intensities) and mean line distance at 250 K and at reference pressure p_0 (see Eq.3.13), $u_e(p, p')$ is the effective amount of absorber (see Eq.3.14), $u_e p_e(p, p')$ is the effective pressure scaled amount of absorber (see Eq.3.15)

As can be seen by easy manipulation, only two combinations of parameters occur in both the Malkmus and Goody statistical band model, that is $A_0 u_e$ and $A_0 B_0 u_e p_e$. Additionally, both models have similar absorption limits. In the weak line approximation (WLA) the optical depth is given by $\delta = A_0 u_e$, while in the strong line approximation (SLA), the expression $\delta = \sqrt{A_0 B_0 u_e p_e}$ is valid. Thus, we can introduce two coefficients ($G_{WLA}(T_0) \equiv A_0$ and $C_{SLA}(T_0, p_0) \equiv \sqrt{A_0 B_0}$) describing the absorption in the limiting cases. The random band model parameters $A(T)$ and $B(T, p)$ for any temperature T and pressure p can be defined in terms of spectroscopic quantities following *Rodgers and Walshaw* [1966]:

$$A(T) = \frac{1}{\Delta v} \sum_l S_l(T) \quad (3.12)$$

$$B(T, p) = \frac{\left(\frac{2}{\Delta v} \sum_l \sqrt{S_l(T) \alpha_l(T, p)}\right)^2}{\frac{1}{\Delta v} \sum_l S_l(T)} \quad (3.13)$$

where Δv is the NBM spectral band width in cm⁻¹. Here we change the units of $S_l(T)$ (line intensity in cm g⁻¹) and of $\alpha_l(T, p)$ (collision half-width in cm⁻¹) because the absorber amounts in the NBM are expressed in terms of g cm⁻². Note that the line structure parameter, $B(T, p)$, is linearly dependent on pressure (see Eq.3.9). In order to convert the line intensities S_l^* (cm molecule⁻¹) from the spectroscopic compilations into intensities S_l (cm g⁻¹) usable for the random band models in the NBM, we use the multiplication factor $N_A/M(m, i)$, where $N_A = 6.022 \cdot 10^{23}$ molecule mol⁻¹ (Avogadro's number) and $M(m, i)$ is the molecular weight of molecule (m) and isotope (i) in g mol⁻¹. The line intensities are scaled with the abundances of the isotopes in the atmosphere.

The diffusivity factor for the five considered gases ($r = 1.66$), which accounts for the zenith angle integration, is included in the absorber amount $u(p, p')$. Temperature variations are taken into account in the effective amount of absorber u_e , defined by:

$$u_e(p, p') = \int_{u(p)}^{u(p')} \Phi(T) du(p'') \quad (3.14)$$

where $u(p, p')$ is the absorber amount in g cm⁻² and $\Phi(T)$ a temperature function, parameterized in Eq.3.16. Temperature and pressure variations along the inhomogeneous paths are computed

Table 3.6: Values of the Vibrational Partition Function $Q_v(T)$ at 204 K, 250 K(= T_0) and 296 K(= T_s) and of the Exponent of the Rotational Partition Function $Q_r(T) = (\frac{T}{T_s})^j$ (after Morcrette [1984]).

Molecule	$Q_v(204\text{ K})$	$Q_v(250\text{ K})$	$Q_v(296\text{ K})$	j
H ₂ O	1.0000	1.0000	1.0000	1.5
CO ₂	1.0214	1.0502	1.0934	1.0
O ₃	1.0080	1.0220	1.0464	1.5
N ₂ O	1.0328	1.0720	1.1277	1.0
CH ₄	1.0002	1.0020	1.0074	1.5

using the pressure scaled amount of absorber $u_e p_e$, defined by:

$$u_e p_e(p, p') = \int_{u(p)}^{u(p')} \frac{p''}{p_0} \Psi(T) du(p'') \quad (3.15)$$

where p_0 is the reference pressure (1 atm) and $\Psi(T)$ a temperature function, parameterized in Eq.3.17. The temperature dependencies of the WLA and SLA absorption coefficients have been parameterized following *Rodgers and Walshaw* [1966]:

$$\Phi(T) = \frac{C_{WLA}(T)}{C_{WLA}(T_0)} = \exp[a(T - T_0) + b(T - T_0)^2] \quad (3.16)$$

$$\sqrt{\Psi(T)} = \frac{C_{SLA}(T, p)}{C_{SLA}(T_0, p)} = \exp[a'(T - T_0) + b'(T - T_0)^2] \quad (3.17)$$

The coefficients of these functions (a, b, d and b') have been determined from $C_{WLA}(=A)$ and $C_{SLA}(=\sqrt{AB})$ at three temperatures: $T_s=296$ K (laboratory temperature), $T_0=250$ K (reference temperature), and $T=204$ K, for each of the 225 NBM spectral intervals. Note that the ratio of the SLA coefficients at different temperatures (Eq.3.17) is independent of pressure.